IEEE Access
Multidisciplinary ⋮ Rapid Review ⋮ Open Access Journal

Received 7 July 2022, accepted 24 July 2022, date of publication 28 July 2022, date of current version 4 August 2022.

Digital Object Identifier 10.1109/ACCESS.2022.3194628

RESEARCH ARTICLE

Reducing Microgrids Integration Complexity in Distribution Networks Considering Bidirectional Power Flow in SFCLs

MOHAMED ELSAMAHY, (Member, IEEE)
University of Saskatchewan, Saskatoon, SK S7N 5A9, Canada
e-mail: mohamed.elsamahy@usask.ca

ABSTRACT In this paper, investigations are carried out to explore the application of the well-known unique bidirectional power flow nature of superconducting fault current limiters (SFCLs) to reduce the complexities of integrating microgrids into distribution networks. More specifically, their adverse impact on the coordination of existing protection of distribution networks, as well as the complexity of setting their internal protection to handle the change in fault current due different modes of operation. In this context, the capability of the proposed SFCL scheme is tested while demonstrating the tandem operation of the utility distribution network and microgrid protection systems and problems related to sensitivity and selectivity are addressed. In addition, different fault contingencies are considered, namely, faults located on the incoming main-lateral connecting the microgrid to the distribution network (where the fault is between the distribution substation protection and the microgrid) and on an adjacent main-lateral from the same main feeder (where the microgrid is located between the distribution substation protection and the fault). Moreover, other faults are located inside the microgrid on a local-line and at a local end-user. Results have shown the efficiency of the proposed SFCL scheme in reducing the short circuit contributions of both the microgrid and the utility network within the coordination limits depending on the direction of flow into the point of connection (PoC). Thus, it allowed a safe continuous integration of microgrids in distribution networks during faulted conditions, while, simultaneously permitted the microgrid to utilize a single protection setting to handle the changes in short circuit current levels when transitioning between grid-connected and islanded modes of operation. The time-domain simulation studies are conducted using PSCAD/EMTDC software.

INDEX TERMS Bidirectional power flow, distribution networks protection, fuse-recloser coordination, microgrids, superconducting fault current limiters (SFCLs).

I. INTRODUCTION

Microgrids are emerging as an important part of the modern distribution networks because they allow the utilities to meet the rapid increase in the load demands without the need to expand the distribution infrastructure [1], [2].

A microgrid can be considered as an entirely DG-based grid with a cluster of local-loads. It is usually connected to the utility grid through a single point, which can either be defined as the point of connection (PoC) or point of common coupling (PCC). The former definition of the connection point will be depicted throughout the investigations of this paper. In addition, a microgrid can operate in either utility grid-connected or islanded modes and interchanges between them seamlessly. To the utility grid, a microgrid behaves as a fully controllable load which at peak hours can even supply power back when operating in grid-connected mode.

Microgrids proven to be effective due to their short construction time, lower capital costs, reduced greenhouse gaseous emissions, reduced transmission power loss (due to the fact that generation is now closer to the loads), improved voltage profile, enhanced reliability and diversification of energy sources. However, integration of microgrids also introduced its own challenges in the context of reliable

The associate editor coordinating the review of this manuscript and approving it for publication was Nagesh Prabhu.

operation of protection systems on the utility distribution grid side (also called utility-grid side) as well as inside the microgrid. [3]–[5].

One major challenge on the utility-grid side is that inclusion of microgrids may compromise the functionality and reliability of the existing protection on the utility-grid side. This is attributed to the microgrid influence on existing distribution networks' short circuit characteristics in terms of: current-flow direction, magnitude and the extent of influence is determined through microgrid size, location of PoC, interconnection methods and type of its local-DGs [6]–[8]. IEEE Std. 1547 [9] was the initial prototype facilitating the immediate disconnection of microgrids and all other distributed generation (DG) units from the distribution network following faults detection. Mainly, to prevent their short circuit current contribution during such stressed events. Many utilities follow the settings of IEEE Std. 1547 as shown in [10] and [11]. This, however, limits the capability of microgrids to enhance the utility-grid supply reliability during stressed contingencies.

On the microgrid side the difficulty arises from the complexity of setting their internal protection systems when transition occurs between the grid-connected and islanded modes of operation [9], [12]–[14]. On one hand, during grid-connected mode the microgrid protection system should respond to both internal-faults as well as faults on the utility-grid side. In the former case, the protection system should isolate the smallest part of the microgrid when clears the fault. While, in the latter case, some fault locations (which affect the voltage sag at the microgrid terminals) dictate that the microgrid should be quickly isolated from the utility-grid if the microgrid contains voltage-sensitive local-loads. In such circumstances, problems that are related to selectivity (such as false, unnecessary tripping (overreaching)) and sensitivity (such as undetected faults or delayed tripping (underreaching) of protection system) may arise. On the other hand, during islanded mode the short circuit current is significantly lower due to the absence of utility-grid short circuit contribution during this mode of operation. Therefore, during such a mode the microgrid protection is accomplished by changing the overcurrent protection settings which should also be coordinated with anti-islanding protection. This procedure itself could be is a challenging task especially when dealing with complex microgrids.

In the context of the above-discussed complexities, the literature contains numerous research work which has been done on the implementation of superconducting fault current limiters (SFCLs) with great focus on the challenges facing the fuse-recloser coordination on the utility-grid side, which arises from integrating microgrids and individual DGs such as [15]–[18]. In addition, the literature also contains almost the same number of research work which has been done on the application of SFCL as well as adaptive overcurrent protection schemes to negotiate the differences in short circuit currents between microgrid grid and islanded mode such as [19]–[24].

Although the microgrid protection is in tandem with utility-grid protection, however, all of the above-mentioned developed SFCL-based solutions were either implemented on the utility-grid side while the microgrid is only represented as lumped DG source, or were implemented inside the microgrid with utility-grid side represented as a lumped source. In different words, these solutions were only tested with either the presence of the utility-grid protection or the presence of the microgrid protection, but not while both protection systems are actively interacting. This brings to light, the need to further investigate the capabilities of the above proposed solutions fully tested during the interacting performance of protection systems, where, problems related to selectivity and sensitivity which may arise. It is worth mentioning that [19] presented only a single case-study showing the tandem operation of both utility-grid and microgrid protection systems during a local fault inside a microgrid, while an SFCL-based scheme installed at PoC.

Based on the previous discussion the contributions of this paper are emphasized in the following points:

1. This paper proposes, through in-depth time-domain simulation studies, the use of the of the unique well-known bidirectional power flow nature in SFCLs to remove the limitation on the microgrid penetration levels connected to distribution systems. In different words, to allow a safe continuous operation of microgrids in distribution networks during faulted contingencies and enhance their supply reliability during such stressed conditions.
2. It also shows the capability of the proposed SFCL to, simultaneously, remove the need for complicated protection settings within microgrids. This is achieved by allowing microgrids protection systems the capacity to utilize a single protection setting to handle the changes in short circuit current levels when transitioning between grid-connected and islanded modes of operation.
3. The paper tests the performance of the proposed SFCL scheme considering the tandem operation of utility-grid and microgrid protection systems during the possible faulted scenarios. In addition, it also addresses the possible selectivity and/or sensitivity problems which may arise during such an interacting protection operation with the presence of the proposed SFCL scheme.

II. SYSTEM UNDERSTUDY

A. DISTRIBUTION NETWORK AND MICROGRID

The same distribution network investigated in [25], and shown in Fig. 1, is also depicted during the investigations of this paper. The backbone of his network contains a substation which serves two 25kV feeders, namely Feeder1 and Feeder2, which are tapped-off at the same point of connection. The system also contains variety of loads such as: constant impedance loads (L1 and L2), composite loads (L3 and L4) and a constant power load (L5). All the loads are

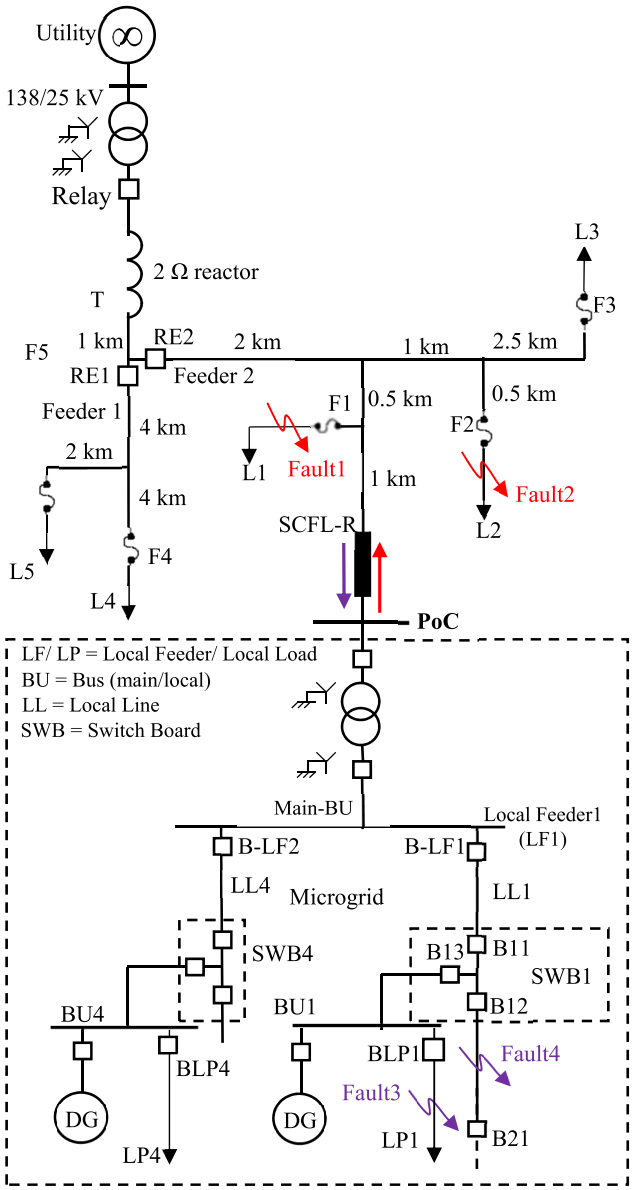

FIGURE 1. Single line diagram of the system understudy.

fuse-protected (F1 to F5). In addition to the utility relay provided in the substation, each of the two feeders is protected by its own head-end recloser, namely, RE1 & RE2. It is worth highlighting that the distribution network is also called utility-grid side during the investigations of this paper.

The same Microgrid structure investigated in [22], also partially shown in Fig. 1, is also depicted during the investigations of this paper and is planned to be integrated to the system understudy at PoC via a 25/13.8 kV interconnecting transformer. The microgrid contains of six local-buses (BU1 to BU6), only Bus1 and Bus4 are shown in in the above figure. In addition, each local-bus is equipped with a local-load, a local-generation and is protected by a switch-board (such as SWB1). Each switch-board consists of a Y-structure three-relayed circuit breakers (such as B11, B12 and B13).

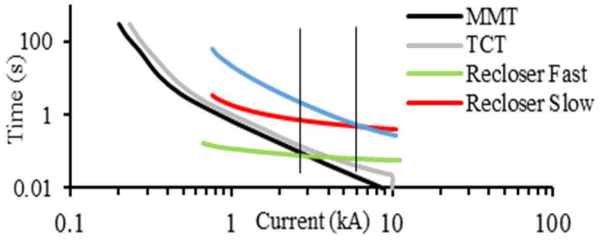

FIGURE 2. Fuse saving protection coordination characteristic curves.

Moreover, the six local-buses are divided equally among two main local-feeders, namely LF1 and LF2.

The microgrid six local-loads (LP1 to LP6), are identical and each of 0.5 MVA, operating at 0.9 power factor and protected by a relayed circuit breaker (such as RLP1). While, the generation at each local-bus consists of five 0.2 MVA synchronous generators operating at a 0.9 power factor and 80% loading condition. The tie-line between the microgrid two main local feeders (between Bus 3 and Bus 6) is normally open.

The data of the understudy distribution network, microgrid as well as the protection setting of both networks are available in the Appendix [22], [25]. The dynamic simulation studies are conducted during the investigations of this paper using the PSCAD/EMTDC software.

B. PROTECTION COORDINATION

For the system understudy, shown in Fig. 1, the head-end recloser of each feeder (such as RE2) will conduct two fast fault-clearing attempts in order to allow temporary faults self-clearance. Following recloser operation, if the fault is still present, the fuse (such as F1) clears the fault. In different words, for all the coordination paths of the system understudy a ''fuse-saving scheme'' is utilized.

This coordinated operation requires the knowledge of the maximum and minimum fault currents for each coordinated protection path from the recloser to the fuse [26]. In addition, the fast characteristic curve of the recloser is placed below the fuse's minimum melting time (MMT), while, the slow characteristic is placed above the fuse's total clearing time (TCT) curve as shown in Fig. 2. This ensures that for a temporary fault the recloser will operate allowing for self-clearing without fuse operation.

For the system under study the maximum short circuit level is limited to 6kA on any coordination path using the 2Ω reactor. While the short circuit levels at fuses under consideration, namely (F1) and (F2), are 4.229 kA and 3.464 kA respectively as will be shown in Section III.

C. FAULT CURRENT LIMITER MODELING

The same resistive SFCL (SFCL-R) model presented in [27], and shown in Fig. 3, is also depicted during the investigations of this paper. This SFCL-R is installed at PoC and is required to have no impact on the steady-state system operation and

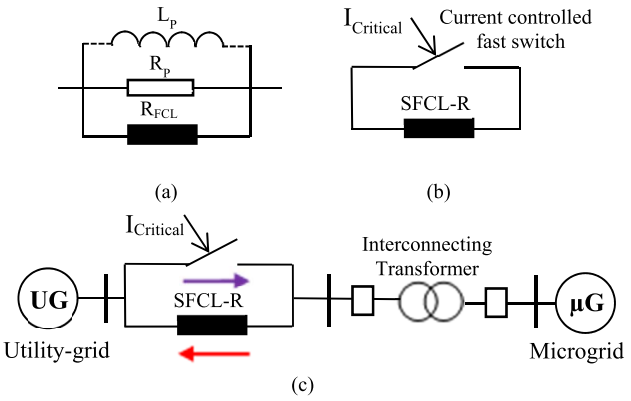

FIGURE 3. Resistive-type SFCL-R under investigations: (a) schematic diagram, (b) PSCAD/EMTDC model and (c) Overall process with SFCL-R installed between utility-grid and microgrid (red & purple directions represent the fault location on utility-grid and microgrid respectively.

exhibit a high resistance during a fault condition to limit the short circuit current.

The transition into the superconducting element state only when its current rises sharply and exceeds its critical value $I_{critical}$ (250 A is selected for the proposed SFCL-R model). As a result, a certain value of resistance is created by self-sensing and self-triggering.

Practically, this SFCL-R is required to limit the fault current between three and five times the rated current ((3 to 5) × I_{rated}). Lower than three, the SFCL is difficult to differentiate a fault from overload current (a large load switching). Greater than five, excessive heating will occur [27]. For the system understudy during the investigations of this paper, the value of SFCL-R is selected through a sensitivity analysis which resulted in a 70 Ω. This is the value which maintains the short circuit current through PoC and SFCL-R within the above-mentioned required level.

It is worth highlighting that the parallel resistance, labeled R_P, is used to protect the FCL from "hot spots" during the transition period and avoid over-voltages in the event that the FCL resistance (R_{FCL}) rises too rapidly. The required switching time for the superconductor element in an SFCL depends on the design, but it typically ranges from a few microseconds to a few milliseconds (5 m.seconds is selected for SFCL-R under study).

III. SIMULATION RESULTS

This section presents the application of the proposed SFCL-R (with its well-known unique bi-directional power flow capability as shown in Fig. 3c) to simultaneously mitigate the challenges arise from the inclusion of microgrids in distribution networks: 1- The adverse impact of microgrid on the utility distribution networks existing protection during faulted conditions. 2- The complexity of setting the microgrid protection systems when transition between grid-connected and islanded modes of operation. 3- Impact of fault location on the microgrid undervoltage protection (of its voltage-sensitive local-loads) while operating in grid-connected mode. Some fault locations cause the microgrid terminal voltage to fall below 0.45 to 0.5 p.u. for three cycles or longer, thus, the microgrid is required to be quickly disconnected from the utility-grid to protect its voltage-sensitive loads.

The investigations conducted during this section are divided into two main parts: The first is Part-A, which presents the adverse impact of microgrid on utility distribution network protection during different faulted conditions. It also highlights the capability of SFCL-R to mitigate such an impact and allow safe continuous connection of the microgrid during these stressed contingencies.

The second is Part-B, which presents the capability of the unique bidirectional nature of the proposed SFCL-R to, simultaneously, allow the microgrid protection system the capacity to utilize a single setting to handle the changes in short circuit current levels when transitioning between grid-connected and islanded modes of operation. During both parts different fault locations are considered on the utility-grid side as well as on the microgrid and problems due to sensitivity and selectivity are highlighted.

A. SFCL-R CAPABIITY TO MITIGATE MICROGRID IMPACT ON DISTRIBUTION NETWORK PROTECTION

The investigations during this part are conducted through the following steps:

1) FINDING MICROGRID PENETRATION LIMITS

During this step the integration location for the microgrid (namely, PoC) is selected as shown in Fig. 1. The same algorithm presented in [6] is then utilized to determine the microgrid penetration limit which will lead to a loss of coordination condition (LCC) when connected at the selected PoC.

The results of this algorithm determined that, for the selected PoC, an LCC first occurs for a microgrid short circuit current levels of 438 A and 395 A during 3-phase and L-L faults respectively. It is worth highlighting, all currents values mentioned during the text of this paper are given in RMS unless otherwise is stated.

2) TESTING UTILITY-GRID PROTECTION W/O SFCL

During this step, the performance of the utility-grid protection system is tested (without and with the microgrid) against the following 3-phase sustained faults: 1- Fault1 is located on the main incoming main-lateral connecting the microgrid to the distribution network (more specifically, on the sub-lateral feeding L1), 2- Fault2 is located on the adjacent main-lateral feeding L2. Throughout the investigations of this paper, fault inception time is at 0.5 seconds of the simulation time.

The investigations start with testing the original performance of the utility distribution network (with the microgrid disconnected) against Fault1 and Fault2 and the time-domain simulation results are presented in Fig. 4 and Table 1 respectively. It can be observed from Fig. 4a and Fig. 4b that the short circuit current experienced by the head-end recloser (RE2) during Fault1 (no microgrid connected) is 4244 A, while, the short circuit current experienced by fuse (F1)

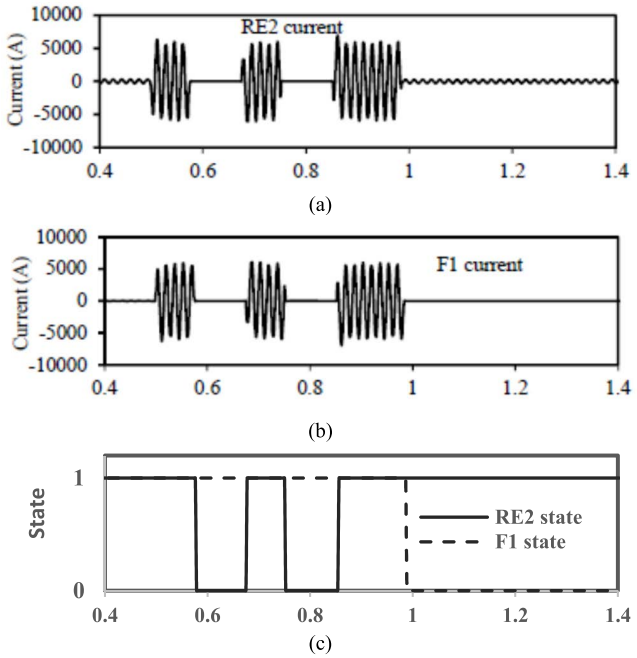

FIGURE 4. Fault1 on the lateral feeding L1 with microgrid disconnected and no SFCL-R: (a) RE2 current, (b) F1 current and (c) RE2 and F1 state signals.

TABLE 1. Results for fault2 with microgrid disconnected.

Equipment	Current (A, RMS)	Time (seconds)
RE2	3479	Attempt1: at 0.58 Attempt2: at 0.76
F1	3461	0.81

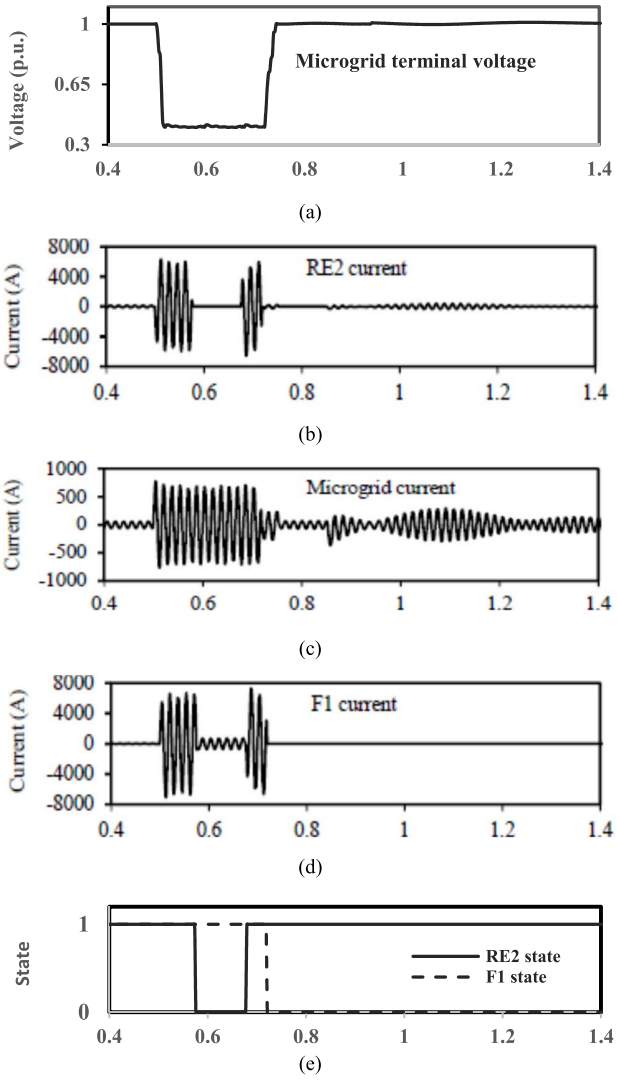

FIGURE 5. 3-phase fault on the lateral feeding L1 with microgrid connected and no SFCL-R: (a) PoC voltage, (b) RE2 current, (c) F1 current and (d) microgrid PoC current, (e) RE2 and F1 state signals.

is 4229 A. The state responses shown in Fig. 4c reveal that RE2 conducted its fast fault-clearing attempts at 0.5762 seconds and 0.7562 seconds of simulation time respectively. Due to the sustained nature of Fault1, F1 finally cleared the fault at 0.9813 seconds. The comparison of RE2 and F1 state response times of Fig. 4c highlights the coordination between RE2 and F1 and the presence a fuse-saving scheme.

On the other hand, during Fault2, RE2 and F2 showed a similar performance to Fig. 4a and Fig. 4b and the values of the experienced fault currents and fault-clearing times are presented in Table 1.

To show the adverse impact of the microgrid on on the existing distribution system protection, therefore, it is now connected at PoC (70Ω SFCL-R is not installed) and Fault1 and Fault2 are then repeated.

The microgrid protection operates in tandem with the utility-grid protection, this results in two microgrid operational scenarios during each fault: During the first scenario, the microgrid contains voltage-sensitive loads, hence, a mandatory disconnection of the microgrid from the system should occur, in the range of 70-160 m.seconds [9], [16].

As result, the microgrid impact on the distribution system protection is automatically eliminated. It worth highlighting that during this fault scenario the microgrid undervoltage protection should be coordinated with its anti-islanding protection. This, however is outside the main scope of this paper.

While, during the second scenario, the microgrid does not contain any voltage-sensitive loads and remains connected to the system during this faulted condition. This scenario is adopted during the remaining investigations of this part and its time-domain simulation results are shown in Fig. 5 and Table 2.

Fig. 5a shows that upon the occurrence of Fault1 (between the microgrid PoC and utility-grid head-end recloser RE2) the voltage at PoC dropped to 0.41 p.u. (below the range 0.45 to 0.5 p.u.) and continued for longer than three cycles. It can also be observed from Fig. 5b that, during Fault1 with the microgrid connected at PoC, RE2 experienced the same short

TABLE 2. Simulation of fault2 with microgrid connected.

	Current (A, RMS)		Clearing Time (Seconds)		PoC voltage (p.u.)	
	w/o SFCL	with SFCL	w/o SFCL	with SFCL	w/o SFCL	with SFCL
RE2 Att.1	3241	3395	0.586	0.5827	-	-
RE2 Att.2			Did not occur	0.7627	-	-
PoC	510	132	-	-	0.59	0.81
F2	3740	3520	0.7439	0.7915	-	-

circuit current of 4244 A compared to its level previously shown in Fig. 4a. This is, however, expected since Fault1 is located between the microgrid and RE2. In addition, the microgrid contributed a current of 530 A to this fault as shown in Fig. 5b.

As a result, the fault current experienced by Fuse (F1) is increased to 4760 A as shown in Fig. 5d (compared to 4229 A as shown in Fig. 4b). RE2 conducted its first fault-clearing attempt at 0.5762 seconds of the simulation time, while, F1 continued to receive the same amount of excess fault current until it removed the fault at 0.7386 seconds (compared to 0.9813 seconds as shown in Fig. 4c). Consequently, RE2 did not conduct its second fault-clearing attempt as shown in Fig. 5e. The comparison of RE2 and F1 response times of Fig. 5e shows that the presence of the microgrid during Fault1 led to an LCC between RE2 and F1 and the fuse-saving scheme is defeated.

On the other hand, during Fault2 on the lateral feeding L2 (adjacent to the microgrid) the voltage at PoC only dropped to 0.59 p.u. and the short circuit current experienced by RE2 is reduced to 3241 A. This is, however, expected due to the fact that the microgrid is located between RE2 and Fault2. Thus, RE2 conducted its first fault-clearing attempt at 0.5886 seconds of the simulation time.

In addition, the short circuit current experienced by F2 is increased to 3740 A, this is also expected due to the microgrid contribution to this fault (i.e. 510 A). F2 finally cleared the fault at 0.7439 seconds, therefore, RE2 did not conduct its second fast fault-clearing attempt. It can be concluded from the above-discussed results (also summarized in Table 2) that the presence of the microgrid not only lead to an LCC between RE2 and F2 (i.e. defeated the fuse-saving scheme), but also caused a reduction in RE2 sensitivity by 8.3 m.seconds compared to its response with the microgrid disconnected.

3) TESTING UTILITY-GRID PROTECTION WITH SFCL

During this step the microgrid is connected at PoC and 70Ω SFCL-R is installed at its terminals. Fault1 and Fault2 are repeated and the time-domain simulation results are presented in Fig.6 and Table 2 respectively. The currents flow through SFCL-R, during these faults, are in the direction from the microgrid towards the utility-grid side.

It can be observed from Fig. 6a and Fig. 6b that during Fault1, the presence of 70Ω SFCL-R limited the microgrid contribution to the fault current to a of 723 A instantaneous peak-value during the first half-cycle from the fault inception time (compared to 752 A instantaneous peak-value of Fig. 5b). The current is further reduced to 137.9 A in the second half-cycle. In different words, the microgrid contribution to the fault is reduced to a value equals to 3.26 times its steady-state current of 42.3 A.

Here again, as expected, the short circuit current experienced by RE2, namely 4244 A, is unchanged. The reduction of the microgrid contribution to the fault is reflected in a reduction of the short circuit current experienced by F1 to 4373 A as shown in Fig. 6d (compared to 4750 A in Fig. 5c). As a result, RE2 conducted its two fast fault-clearing attempts at 0.5762 seconds and 0.762 seconds, hence, F1 finally cleared Fault1 at 0.9531 seconds as shown in Fig. 6e (compared to 0.7386seconds in Fig. 5e). The comparison between the state responses in Fig. 5e and Fig. 6f reveals that the presence of 70Ω SFCL-R restored the coordination between RE2 and F1 on the utility-grid side with the presence of the microgrid. The presence of 70Ω SFCL-R also improved the voltage-sag at PoC to a minimum value of 0.66 p.u. as shown in Fig. 6f.

On the other hand, during Fault2, where the microgrid is located between the fault and the utility-grid protection, the presence of the 70Ω SFCL-R maintained the voltage-sag at PoC at 0.81 p.u.. The short circuit current experienced by RE2 during this fault is 3395 A, while the short circuit current experienced by Fuse F2 is 3520 A (compared to 3740 A of Table 2). The excess current experienced by F2 during this fault is attributed to the reduced value of the microgrid contribution to the same fault (132 A). RE2 conducted its two fault-clearing attempts at 0.5827 seconds and 0.7627seconds respectively. F2, finally, cleared the fault at 0.7915 seconds. These response times reveal that 70Ω SFCL-R, once again, restored the coordination between RE2 and F2 on the utility-grid side and allowed a safe continuous connection of the microgrid during Fault2.

B. SFCL-R CAPABIITY TO ALLOW SAME PROTECTION-SETTING DURING ALL MICROGRID OPERATION MODES

The investigations conducted during this part presents the capability of 70Ω SFCL-R to permit the microgrid the ability to utilize a single protection setting during all of its operating modes. The investigations during this part are conducted through the following steps:

1) SELECTING A MICROGRID SETTING

During this step a microgrid protection setting is firstly selected to be utilized during all the forthcoming investigation steps. This is the setting which is normally utilized against phase-faults during islanded mode.

The normal performance of the selected setting (during islanded mode) is then tested against the following sustained

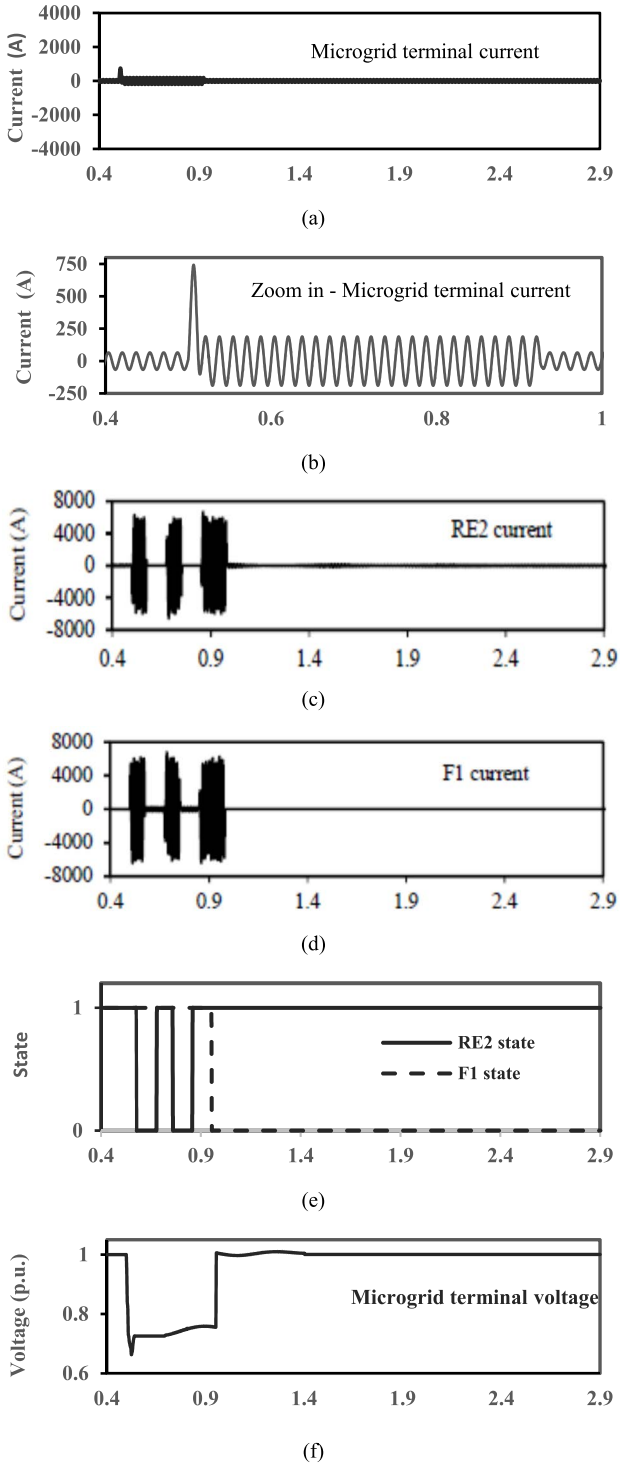

FIGURE 6. 3-phase fault at load L1 with a microgrid connected at PoC and a 70Ω SFCL-R is connected: (a) microgrid PoC current, (b) zoom in the microgrid PoC current, (c) RE2 current, (d) F1 current, (c) (e) RE2 and F1 state signals, (f) Microgrid PoC voltage.

L-L faults: 1- Fault3, is located at local-end user (LP1) which is primarily protected by (RLP1). 2- Fault4 is located on microgrid local-line2 (LL2) which is primarily protected by

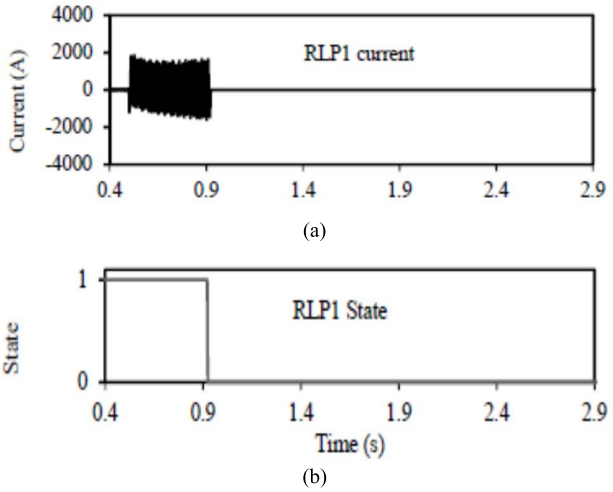

FIGURE 7. L-L fault at LP1 with a microgrid in islanded-mode: (a) RLP1 current and (b) RLP1 state signal.

TABLE 3. Simulation of fault4 with microgrid connected.

	Islanded mode		Gird connected mode w/o SFCL		Gird connected mode with SFCL	
	Current (A, RMS)	Time (Sec)	Current (A, RMS)	Time (Sec)	Current (A, RMS)	Time (Sec)
RE2 Att.1	-	-	2165	0.6285	214	Did not occur
RE2 Att.2				Did not occur		
PoC	-	-	2150	-	198.4	-
F2	702	1.14	4596	0.7393	1061.4	1.004

(B12). The simulation results are presented in Fig. 7 and Table 2.

Fig. 7a shows that the short circuit current experienced by RLP1, following the inception of Fault3 is 945.5 A. Thus, RLP1 removed the fault at 0.9387 seconds of simulation time as shown in Fig. 7b. On the other hand, during Fault4, B12 experienced a fault current of 702 A, hence, it removed the fault at 1.14 seconds.

2) SELECTED SETTING IN GRID-CONNECTED MODE

During this step, 70Ω SFCL-R is not installed and the microgrid is operating in grid-connected mode while is being protected by same setting selected in step (1). Same Fault3 and Fault4 are repeated and the time-domain results of these faulted scenarios are presented in Fig. 8 and Table 3 respectively.

Fig. 8a shows that during Fault4, RE2 experienced a short circuit current of 1768 A. The utility-grid contribution to this fault (current at PoC) and the short circuit current experienced by RLP1 are 1753 A and 4075.1A respectively as shown in Fig. 8b and Fig. 8c. As a result, a selectivity problem between RE2 and RLP1 is introduced as shown in Fig. 8d. This is because RE2 conducted an unnecessarily fault-clearing

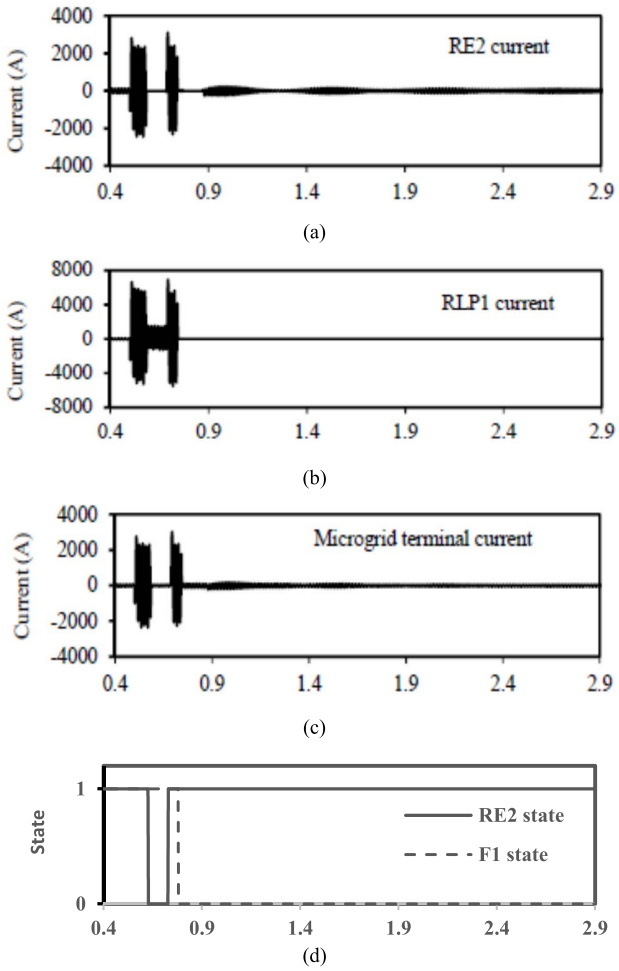

FIGURE 8. L-L fault at LP1, grid-connected mode and w/o SFCL-R: (a) RE2 current, (b) microgrid PoC current, (c) RLP1 current and (d) RE2 and RLP1 state signals.

attempt in its fast-mode at 0.6328 seconds before RLP1 removed the fault at 0.7513 seconds (compared to 0.9387 seconds of Fig.7b).

On the other hand, during Fault4, the short circuit current experienced by RE2, utility-grid contribution to the fault and short circuit current experienced by B12 are 2165 A, 2153 A and 4596 A respectively. This also led to another unnecessary tripping of RE2 at 0.6285 seconds. Then, B12 removed the fault at 0.7393 seconds (compared to 1.14 seconds during the islanded mode). The early tripping of B12 is due to a high short-circuit current supplied by the utility-grid.

3) SELECTED SETTING IN GRID-CONNECTED MODE AND SFCL

During this step, 70Ω SFCL-R is installed at PoC. Here again, the microgrid is operating in grid-connected mode, while is being protected by the same setting selected during step (1). Same Fautl3 and Fault4 are again repeated and the time domain simulations are presented in Fig. 9 and Table 2.

The fault currents flowing through 70Ω SFCL-R are in the direction from the utility-grid to the microgrid.

It can be observed from Fig. 9a, the short circuit current experienced by RE2 during Fault3 is reduced to a value of 176 A due to the presence of 70Ω SFCL-R. This value is below its fast-mode phase pickup setting (400 A), therefore, its unnecessary attempt to clear Fault3 is prevented. Fig. 9b and 9c also show, during the same fault, the presence of 70Ω SFCL-R also limited contribution of the utility-grid to the fault to 163 A within the second half-cycle from the fault inception time.

In different words, the current experienced at PoC is limited to 3.86 times of its steady-state value. As a result, the short circuit current experienced by RLP1 is 1235.7 A and it removed the fault at 0.9088 seconds as shown in Fig. 9e (compared to 0.7513 seconds as shown in Fig. 7b).

The comparison of RE2 and F1 state responses in Fig. 7b, Fig. 8d and Fig. 9e reveals that the presence of 70Ω SFCL-R allowed the microgrid to utilize the same single protection setting to handle the changes in short circuit currents during Fault3 when transitioning between grid-connected and islanded modes of operation.

On the other hand, during Fault4 with microgrid is in grid-connected mode and 70Ω SFCL-R is installed, the short circuit current experienced by RE2, the utility-grid contribution to the fault and fault current experienced by B12 are 212.4 A, 198.4 A and 1061 A respectively. Once again, the circuit current experienced by RE2 is below its phase pickup setting fast mode (400 A), therefore, its unnecessary attempt to clear Fault2 is prevented.

Finally, B12 removed the fault at 1.004 seconds. This reveals that the presence of 70Ω SFCL-R allowed the microgrid to utilize the same single protection setting to handle the changes in short circuit currents during Fault4 when transitioning between grid-connected and islanded modes of operation.

It is worth mentioning that the performance of the backup protection of LL1 (namely, B11) was also tested during this step, while increasing the size of the DG sources connected at BU1. Test cases considered four levels of generation size increment, namely, 5%, 10%, 15% and 20%.

During these cases, B12 was made to fail-to-trip for Fault4 in order to allow B11 to take a backup action. The increase in generation size led to a reduction of the fault current seen by B11 (from its original value of 1061.4 A) by 7 A, 15.6 A, 23.4A and 31.2 A.

In addition, the performance of B11 experienced a delay-time. This delay was labeled as ‘‘adverse’’ only if: trip time of backup protection B11 is longer than the normal trip-time of the primary protection B12 (during grid-connected mode with SFCL-R installed) plus 3 cycles backup-action delay. Namely, 1.0041 seconds = 1.0041 seconds (as shown in Table 3) + 0.05 seconds. The adverse delay-time only appeared at 15% and 20% increase of the generation size at BU1, where B11 cleared the fault during these two cases at 1.065 seconds and 1.0593 seconds respectively.

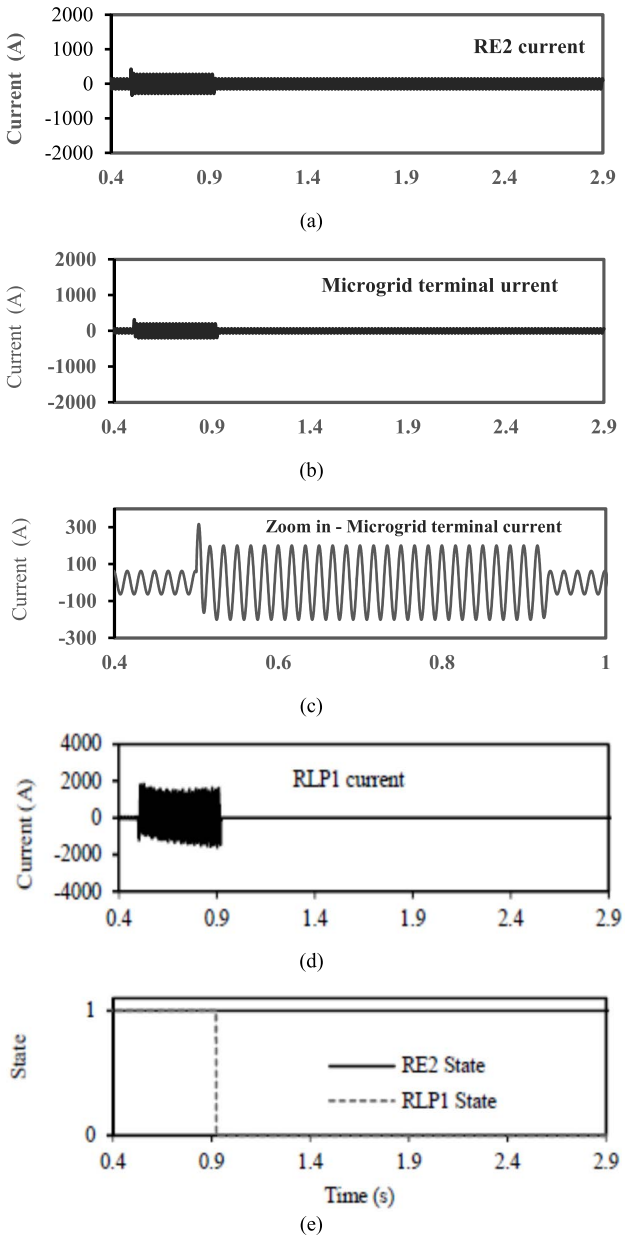

FIGURE 9. L-L fault at LP1, grid-connected mode and with SFCL-R connected: (a) RE2 current, (b) microgrid PoC current, (c) zoom on the microgrid PoC current, (d) RLP1 current and (e) RE2 and RLP1 state signals.

Due to space limitation, Authors of this paper will carry out additional investigations, in a subsequent paper, to explore the impact of delayed trip-action of microgrid local-line backup protection (such as B11) on the continuous connection of the synchronous DGs connected at nearby buses. More specifically, for the cases where synchronous DGs with low inertial exist, an attention will be directed to coordination issues between the microgrid and the DG protection.

IV. COMPARISON WITH SCHMES FROM LITERATURE

In this section the 70Ω SFCL-R scheme proposed in this paper is compared to some other proposed technologies presented in the literature, namely, [25], [22] and [19] respectively. This comparison is conducted to highlight the robustness and efficacy 70Ω SFCL-R as well as its compliance with IEEE 1547 standard [9] and NERC regulations [28].

The comparison is conducted based on the following points: 1- The structures of the proposed schemes considering complexities and similarities. 2- The efficiency of protection performances and vulnerabilities during some selected faulted case scenarios, namely, Fault1 and Fault3 which are previously described in Subsection III-B.

A. COMPARISON WITH A COMMUNICATION-ASSISTED SCHEME [25]

In this subsection, the protection scheme which is proposed in [25], named as R_D, is tested against same Fault1 discussed earlier in this paper (between the microgrid PoC and utility-grid head-end recloser RE2), then the results of this test are compared to the performance of 70Ω SFCL-R presented in Fig. 6.

1) STRUCTURE COMPLEXITY & APPLICATION VALIDITY

- The structure of the scheme R_D [25] can be summarized as follows:

- Its a communication-assisted reclosing scheme to mitigate the impact of DGs/Microgrids penetrations to distribution systems. More specifically, it disconnects the microgrid/DG upon fault occurrence, then transfer it to a variable load bank (Z_{RE}) until the fault removal then it reconnects the microgrid/DG back into the system.
- R_D employs a communication and control unit (CCU), variable load bank (Z_{RE}), two thyristor-based circuit breakers (TBCB) and a dedicated recloser at the point of common coupling (PCC).
- The CCU contains both the receiver/transmitter (R/T) unit and the control component of the DG recloser (DG-RC). The communication between the feeder head-end recloser and CCU utilizes Ethernet Fiber Links with a delay time of 5 milliseconds.
- It is also mandatory to conduct a sensitivity study to decide the possible microgrid load sharing conditions and their corresponding current contributions during the faulted conditions (i.e the corresponding pickup values in the CCU, hence determine the corresponding pre-fault loading impedance value from the (Z_{RE}) load bank.

2) PROTECTION PERFORMANCES

- The performance of the scheme R_D proposed in [25] in response to Fault1 (between the microgrid PoC and utility-grid head-end recloser RE2) can be described as follows:

- R_D was capable of disconnecting the microgrid from the distribution system after verifying the following four signals: 1- An instantaneous local tripping signal when the DG terminal current exceeded 105.75 A ($= 2.5 \times I_{MG-F.L}$), 2- A delayed remote fault tripping signal received from the head-end recloser at 0.5004 seconds. 3&4- Two control signals to the load-bank (Z_{RE}) to

select the value of the transfer impedance and another control signal to close the circuit break (normally open) which connects the selected transfer impedance Z_{RE} at the PCC. Finally, the microgrid was fully disconnected at 0.514 seconds, this can be observed from Fig. 11a.

- Upon the fast disconnection of the microgrid, the feeder head-end recloser (RE2) experienced a short circuit current of 4242 A and it conducted its two fault clearing attempts at 0.5770 seconds and 0.7565 seconds respectively. The short circuit current experienced by F1 reached a level of 4226 A, then, finally cleared the fault at 0.983 seconds. Both RE2 and F1 state signals are shown in Fig. 10a.

- It is worth highlighting that the presence of the communication-assisted scheme (R_D) of [25] allowed the fast disconnection of the microgrid in a less than 2 seconds in compliance with IEEE 1547 [9]. However, it allowed a voltage drop at PoC to 0.82 p.u. before the full disconnection of the microgrid from the system. In addition, upon the fault inception, an overshoot in frequency of 1.8 p.u was detected when the scheme disconnected the microgrid from the system and connected it to the Z_{RE} at 5.014 seconds as shown in Fig. 10.b. Moreover, upon fault removal, another overshoot in frequency of 1.02 p.u was also detected when the scheme R_D disconnected the microgrid from Z_{RE} and reconnected it back to the distribution system as shown in Fig. 10.c. Both overshoots decayed to the nominal frequency.

- The comparison between the performance of scheme (R_D) discussed above and the performance of the 70Ω SFCL-R scheme presented in Fig. 6 can be summarized in the following points:

- Although the scheme (R_D) proposed in [25] showed effectiveness in fully mitigating the impact of the microgrid via disconnecting it in manner in compliance with IEEE 1547 [9], however, the scheme performance also contains a performance vulnerability in the case of the failure of its communication link.
- The scheme (R_D) disconnected the microgrid upon fault occurrence, then, transferred it to an auxiliary impedance in order to emulate the pre-fault loading condition, for the purpose to speed up and secure the resynchronization process after fault removal. However, the frequency overshoot resulted during its performance in response to Fault1 is outside the frequency override limits presented by [28]. The brings into light the need to continuously monitor the synchronization process.
- The performance of the 70Ω SFCL-R, proposed in this paper, permitted the continuous connection of the microgrid to the distribution system during the faulted condition in compatible with NERC voltage ride through regulations [28]. More specifically, it maintained a voltage drop of 0.76 p.u. at PoC. Thus, the microgrid contributed to enhance the power supply reliability on the feeder during the stressed contingency.

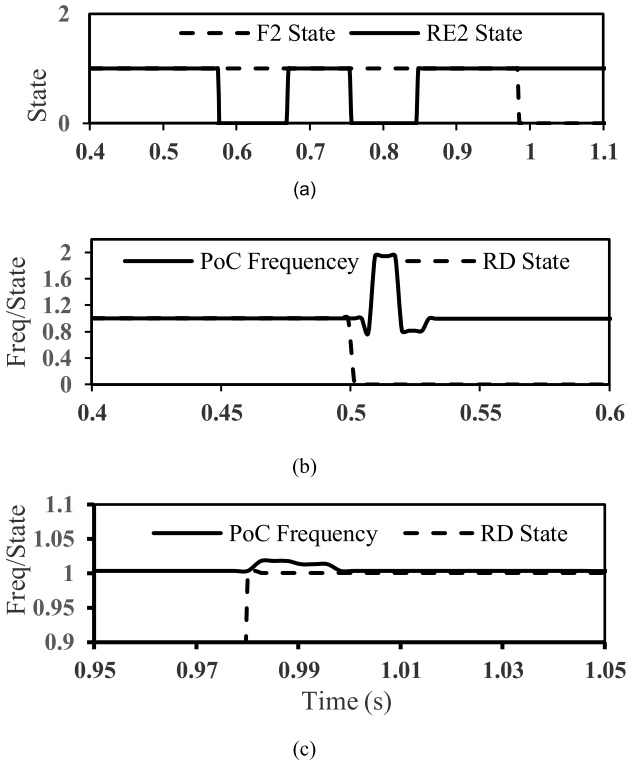

FIGURE 10. 3-phase fault at load L1 with a microgrid connected at PoC and a Recloser scheme (R_D) of [25] is connected: (a) RE2 and F1 state signals, (b) Zoom on the microgrid PoC frequency and (RD) state signal at fault inception, (b) Zoom on microgrid PoC frequency and (RD) state at fault removal.

B. COMPARISON WITH AN ADAPTIVE HYBRID MICORGRID PROTECTION SCHEME [22]

In this subsection, the protection scheme which is proposed in [22] is tested against same microgrid internal Fault3 (located at local-end user (LP1) in the microgrid). The results of this test are, then, compared to the performance of 70Ω SFCL-R presented in Fig. 9.

1) COMPLEXITY & APPLICATION VALIDITY

- The structure of the scheme proposed in [22] can be summarized as follows:

- This scheme employs adaptive overcurrent and differential protection simultaneously in order to manage the required change in the microgrid short circuit current characteristics following the transition between grid and islanded operation modes.
- The scheme determines the microgrid mode of operation from the utility substation via a communication link between the feeder head-end recloser and the interconnecting breaker.
- The differential relays are used to protected individual lines and interconnecting load buses. Therefore, they require communication channels between the ends of each protection zone.

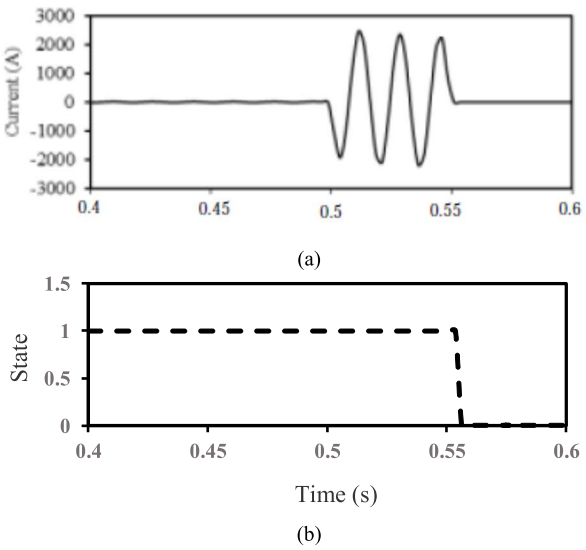

FIGURE 11. L-L fault at LP1, grid-connected mode and the hybrid adaptive scheme of [22] is also connected: (a) RLP1 current, (b) RPL1 state signal.

- The adaptive overcurrent relays are used to protect each individual load point and settings are adjusted to the mode of the microgrid. The mode of the microgrid is transmitted to these adaptive overcurrent relays through the use of a communication channels between the interconnecting breaker (between the utility and the microgrid) and each load point relay. These adaptive over current relays are considered instantaneous.

2) PROTECTION PERFORMANCES

- The performance of the scheme hybrid scheme proposed in [22] in response to Fault3 (located at local-end user (LP1)) can be described as follows:

- While the microgrid in grid-connected mode, the adaptative overcurrent protection relay (of the scheme proposed in [22]) experienced a current of 1245 A as shown in Fig. 11a. This relay was capable to trip at 0.556 seconds (= 0.042 seconds operation delay + 0.014 seconds communication and circuit breakers operation delays) as shown in Fig. 11b. In order to confirm the coordination with the differential protection relay part the following records were also observed: the values of the differential and restraining currents were 0.000576 p.u and 1.8 p.u. respectively and no trip signal was detected.
- While the microgrid in islanded mode, the adaptative overcurrent protection relay (of the scheme proposed in [22]) experienced a current of 956 A. In addition, this relay was capable to trip at 0.552 seconds (= 0.038 seconds operation delay + 0.014 seconds communication and circuit breakers operation delays). In order to confirm the coordination with the differential protection relay part the following records were observed: the values of the differential and restraining currents were 0.00068 p.u and 2.1 p.u. respectively and no trip signal was detected.

- The comparison between the performance of the hybrid scheme presented in [22] and the performance of the 70Ω SFCL-R scheme shown in Fig. 9 can be summarized in the following points:

- The scheme proposed in [22] showed effectiveness in managing the change of the microgrid protection setting during the transition between grid-connected and islanded mode of operations. However, the scheme performance is yet vulnerable due to inherent dependability of the scheme operation on the communication links.
- During the performance of scheme proposed in [22], there is continuous need to confirm the coordination between the two different algorithms of the adaptive overcurrent and differential protection relay.
- As presented in Fig. 9, the 70Ω SFCL-R showed a robust and sustainable performance in allowing the microgrid to utilize the same protection setting during the transition between different modes of operation.

C. COMPARISON WITH A SIMILAR FCL SCHEME

In this subsection, the protection scheme which is proposed in [19] is tested against the same Fault1 (between the microgrid PoC and utility-grid head-end recloser RE2), as well as, same microgrid internal Fault3. The results of these tests are, then, compared with the performance of the 70Ω SFCL-R scheme proposed in this paper as presented in in Fig. 6. and Fig. 9.

1) COMPLEXITY & APPLICATION VALIDITY

- The FCL scheme presented in [19] utilize the same well-established principle of bi-directional self-triggering of superconducting fault current limiters.

- However, there was no mention in [19] of the design settings, namely, the critical current and the state transition time. Therefore, for the purpose of testing the protection performance of this scheme, its parameters were also set to a critical current of 250 A and a state transition time of 5 m.seconds.

2) PROTECTION PERFORMANCES

- The performance of the scheme proposed in [19] in response to Fault1(between the microgrid PoC and utility-grid head-end recloser RE2) can be described as follows:

- The scheme allowed the safe continuous connection of the microgrid to the distribution system during this faulted condition. In this context, it limited the microgrid contribution to the fault current to 700 A, then, further reduced this value to 257 A (= 6.075 × $I_{MG-F.L}$, where $I_{MG-F.L}$ = 42.3 A) after one complete cycle from fault inception time, and maintained this current value for another 4 complete full cycles. The scheme further reduced the microgrid contribution to the fault current to 180 A (= 4.26 × $I_{MG-F.L}$, where $I_{MG-F.L}$ = 42.3 A)

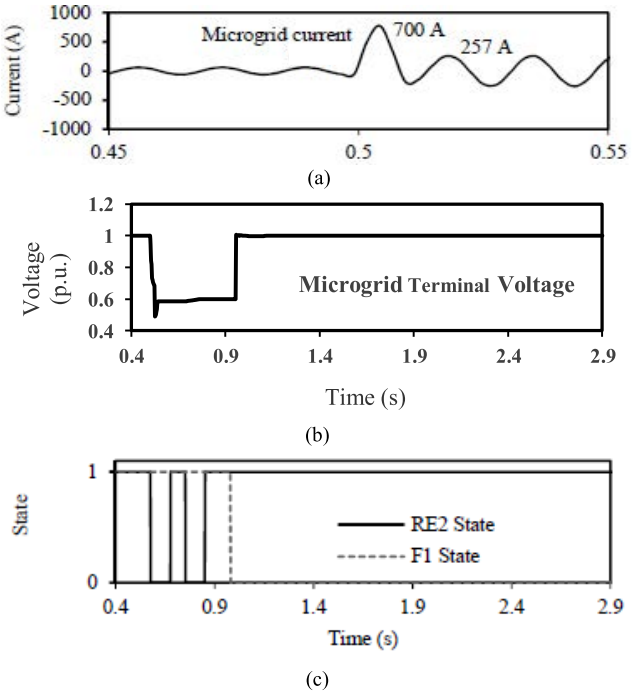

FIGURE 12. 3-phase fault at load L1 with a microgrid connected at PoC and a Recloser scheme of [25] is connected: (a) microgrid PoC current, (b) microgrid terminal voltage, and (c) RE2 and F1 state signals.

after 5 cycles from the fault inception time as shown in Fig. 13a.

- According to [27], these current values (700 A and 257 A) are greater than 5 × $I_{MG-F.L}$ which makes the scheme proposed by [19] vulnerable to excessive heating during these 5 full cycles as shown in Fig. 12.a.
- It is worth mentioning, PoC experienced a voltage drop of 0.49 p.u. for complete five cycles from fault inception time, then, this voltage drop increased to 0.586 p.u. as shown in Fig. 12.b. This voltage drop is outside the voltage ride through range presented in [28].
- RE2 experienced a short circuit current of 4242 A, while F_1experienced 4423 A and finally cleared the fault at 0.9489 seconds as shown in Fig. 12c.

- The performance of the scheme proposed in [19] in response to Fault3 (located at local-end user (LP1)), while the microgrid was in grid-connected mode can be describe as follows:

- The presence of FCL of [19] allowed the microgrid to maintain its same islanded mode protection setting. More specifically, it reduced the the utility contribution to fault on the microgrid side to a value of 289 A in the first half cycle from fault inception time then furtherly reduced this value to 249 during the next half cycle as shown in Fig. 13a.
- Here again, these two current values (289 A and 249 A) are greater than 5 × $I_{MG-F.L}$) which makes the scheme proposed by [19] vulnerable to excessive heating.

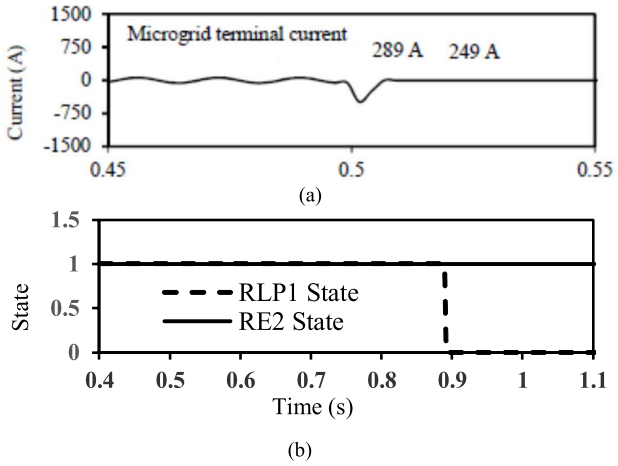

FIGURE 13. 3-phase fault at load L1 with a microgrid connected at PoC and a Recloser scheme of [25] is connected: (a) microgrid PoC frequency and recloser scheme state signal at fault inception, (b) microgrid PoC frequency and recloser scheme state after fault removal.

- The short circuit current experienced by RE2 to a value of 176 A, therefore, its unnecessary attempt to clear Fault3 is prevented. Finally, the short circuit current experienced by RLP1 is 1276.5 A and it removed the fault at 0.8982 seconds as shown in Fig. 13b.

The comparison between the performances of the FCL proposed by [19] and the performance of the 70Ω, SFCL-R presented in Fig. 6 and Fig. 9 can be summarized in the following points:

- Both schemes were able to mitigated the impact of the microgrid on the distribution system, meanwhile, allowed the continuous operation during the faulted condition. In addition, the two schemes showed capability to allow the microgrid to maintain the same protection setting during different modes of operation.
- However, during all test cases, the FCL scheme of [19] showed vulnerability to excessive heating due to its lack of ability to reduce its current to values less than 5 × $I_{MG-F.L}$ during these test cases.

V. CONCLUSION

This paper introduces investigations on the application of the well-known unique bidirectional power flow nature SFCLs to reduce the complexity of integrating microgrids to distribution networks.

In terms of secured operation of utility-grid protection with continuous presence of microgrids during faulted conditions (current flows from microgrid to utility-grid side), results have shown that 70Ω, resistive-type SFCL (SFCL-R) reduced the microgrid contribution to 26.01% of its value without SFCL-R (equals 3.26 times of its steady-state value) when the fault is located between the microgrid and the utility-grid protection. On the other hand, when the microgrid is located between the fault and the utility-grid protection a reduction of 25.88% (equals 3.12 times of its steady-state

value) is obtained. These reductions occurred within the second half cycle from fault inception time and improved the time-responses of the utility-grid primary local-protections at the faults by 0.215 and 0.048 seconds respectively according to the fault location.

In terms of the reliability and reduced complexity of microgrid protection systems, the results have shown that 70Ω, SFCL-R granted the microgrid the capacity to utilize the same single protection setting to handle the changes in microgrid short circuit currents while transitioning between grid-connected and islanded modes of operation. More specifically, results have shown that 70Ω, SFCL-R reduced the utility-grid contribution to 7.57% of their values without SFCL-R when the fault is located at a local-end user. On the other hand, when the fault is on a microgrid local fault, results have shown that 70Ω, SFCL-R reduced the utility-grid contribution to the fault to 9.23%. These reductions occurred within the second half cycle from fault inception time and they improved the time-responses of the microgrid primary local-protection at the faults by 0.1695 and 0.2647 seconds according to the fault location, hence, prevented unnecessary fault clearing attempts by utility grid head-end recloser.

The structure and the efficacy of performance of the 70Ω, SFCL-R proposed in this paper were also compared to some other schemes proposed in the literature, namely in [25], [22] and [19]. The comparison is conducted based on two points: The first is the complexity of structures, utilized technologies and similarities. While, the second is the efficiency of protection performances and vulnerabilities were also compared during the faulted case scenarios. The structure comparison highlighted the technical and economic challenges against the practical application of the other schemes proposed in [25] and [22] while it showed the structure similarity with the scheme proposed in [19]. On the other hand, the performance comparison highlighted the robustness and sustainability of the 70Ω, SFCL-R, this is in comparison to dependability of operation on the communication links, additional coordination checks between different protection algorithms of the same scheme, voltage and frequency overrides incompliance and vulnerability to excessive heating of the schemes proposed in [25], [22], and [19] respectively.

It is worth highlighting that the value of SFCL-R (70 Ω) and the results presented in this paper are based on the system understudy, therefore, it is paramount to conduct a sensitivity analysis to select the type and the value of SFCL that guarantees the suitability of the proposed approach for a certain case-study.

This paper also brought to consideration two future research points regarding the investigated application of SFCL-R: The first is concerned with addressing the coordination of the microgrid undervoltage and anti-islanding protection during different grid-connected mode stressed contingencies. While, the second is concerned with coordination issues between microgrid and local synchronous DG protections which may result from delayed fault-tripping of the backup protection of microgrids local-lines. These two research points are currently in investigation stage and the results will be reported in a subsequent publication''

APPENDIX

A. UTILITY-GRID PROTECTION

1- Head-end recloser (RE2): ABB PCD2000 CT: 600/5, Phase trip: 400 A, Fast curve: ANSI INV INST-1, Slow curve: ANSI INV-2. 2-Fuses (F1 & F2): S&C SM4,5 slow, 25kV, 200E&175E.

TABLE 4. Conductor data.

Conductor	R_1, Ω/KM	L_1, Ω/km	C_1, μS/km	R_0, Ω/km	L_0, Ω/km
Tulip	0.173	0.291	5.848	0.4996	0.84
Pigeon	0.339	0.323	5.405	0.979	0.933
Raven	0.536	0.342	5.102	1.548	0.988

B. MICROGRID PROTECTION

1- Local-lines and local-loads protection (B12 & RLP1): ABB PCD2000 CT: 150/5, phase pickup: 175A, 240A, ANSI INV2&1.5 respectively. 2-The pickup values are calculated in accordance with the same procedure presented in [22].

TABLE 5. SFCL-R model parameters.

SFCL-R	Parameters
$I_{critical}$	250 A
Switching time (insertion time)	5 m.seconds
Maximum allowable duration (removal time)	5 s

REFERENCES

[1] I. Waseem, M. Pipattanasomporn, and S. Rahman, ''Reliability benefits of distributed generation as a backup source,'' in *Proc. IEEE Power Energy Soc. Gen. Meeting*, Jul. 2009, pp. 1–8.

[2] A. D. T. Le, M. A. Kashem, M. Negnevitsky, and G. Ledwich, ''Distributed generation diversity level for optimal investment planning,'' in *Proc. AUPEC*, Melbourne, VIC, Australia, 2006, pp. 1–9.

[3] M. R. Islam and H. A. Gabbar, ''Analysis of microgrid protection strategies,'' in *Proc. Int. Conf. Smart Grid (SGE)*, Aug. 2012, pp. 1–6.

[4] H. Nikkhajoei and R. H. Lasseter, ''Microgrid protection,'' in *Proc. IEEE Power Eng. Soc. Gen. Meeting*, Jun. 2007, pp. 1–6.

[5] T. K. Abdel-Galil, A. E. B. Abu-Elanien, E. F. El-Saadany, A. Girgis, Y. Mohamed, M. M. Salama, and H. Zeineldin, ''Protection coordination planning with distributed generation,'' CANMET Energy Tech. Center, Varennes, QC, Canada, Tech. Rep. CETC-Varennes 2007-149 (TR), 2007, pp. 1–197.

[6] K. A. Wheeler, S. O. Faried, and M. Elsamahy, ''Assessment of distributed generation influences on fuse-recloser protection systems in radial distribution networks,'' in *Proc. IEEE/PES Transmiss. Distrib. Conf. Expo. (T&D)*, May 2016, pp. 1–5.

[7] H. Yazdanpanahi, W. Xu, and Y. W. Li, ''A novel fault current control scheme to reduce synchronous DG's impact on protection coordination,'' *IEEE Trans. Power Del.*, vol. 29, no. 2, pp. 542–551, Apr. 2014.

[8] W. El-Khattam and T. S. Sidhu, ''Restoration of directional overcurrent relay coordination in distributed generation systems utilizing fault current limiter,'' *IEEE Trans. Power Del.*, vol. 23, no. 2, pp. 576–585, Apr. 2008.

[9] *Interconnecting Distributed Resources with Electric Power Systems*, Standard 1547, 2003.

[10] *Generation Interconnection Requirements at Voltages 34.5 kV and Below*, SaskPower, Regina, SK, Canada, Mar. 2005.
[11] *Interconnection Requirments for Power Generators 35kV and Below*, BChydro, Vancouver, BC, Canada, May 2010.
[12] N. A. Mohamed and M. M. A. Salama, "A review on the proposed solutions to microgrid protection problems," in *Proc. IEEE Can. Conf. Electr. Comput. Eng. (CCECE)*, May 2016, pp. 1–5.
[13] S. Chowdhury, S. P. Chowdhury, and P. Crossley, "Microgrids and active distribution networks," *IET Renew. Energy Ser.*, vol. 6, pp. 1–321, Jan. 2009.
[14] H. Zeineldin, E. El-saadany, and M. A. Salama, "Distributed generation micro-grid operation: Control and protection," in *Proc. Power Syst. Conf., Adv. Metering, Protection, Control, Commun., Distrib. Resour.*, Mar. 2006, pp. 105–111.
[15] F. G. K. Guarda, G. Cardoso, C. D. L. da Silva, and A. P. de Morais, "Fault current limiter placement to reduce recloser—Fuse miscoordination in electric distribution systems with distributed generation using multiobjective particle swarm optimization," *IEEE Latin Amer. Trans.*, vol. 16, no. 7, pp. 1914–1920, Jul. 2018.
[16] K. Wheeler, M. Elsamahy, and S. Faried, "Use of superconducting fault current limiters for mitigation of distributed generation influences in radial distribution network fuse–recloser protection systems," *IET Gener., Transmiss. Distrib.*, vol. 11, no. 7, pp. 1605–1612, May 2017.
[17] B. Li, C. Li, F. Guo, and Y. Xin, "Overcurrent protection coordination in a power distribution network with the active superconductive fault current limiter," *IEEE Trans. Appl. Supercond.*, vol. 24, no. 5, pp. 1–4, Oct. 2014.
[18] M. H. Kim, S. H. Lim, J. F. Moon, and J. C. Kim, "Method of recloser-fuse coordination in a power distribution system with superconducting fault current limiter," *IEEE Trans. Appl. Supercond.*, vol. 20, no. 3, pp. 1164–1167, Jun. 2010.
[19] K. A. Wheeler and S. O. Faried, "Bi-directional use of fault current limiters for microgrid integration and protection," in *Proc. IEEE Electr. Power Energy Conf. (EPEC)*, Oct. 2019, pp. 1–6.
[20] P. McGuckin and D. Wang, "Enhanced protection selectivity in LVDC networks using a superconducting resistance," in *Proc. IEEE 3rd Int. Conf. DC Microgrids (ICDCM)*, May 2019, pp. 1–5.
[21] L. Chen, H. Chen, G. Li, Y. Xu, L. Ren, and Y. Tang, "Application of a resistive type superconducting fault current limiter for a DC microgrid system," in *Proc. IEEE Int. Conf. Appl. Supercond. Electromagn. Devices (ASEMD)*, Apr. 2018, pp. 1–2.
[22] K. A. Wheeler, S. O. Faried, and M. Elsamahy, "A microgrid protection scheme using differential and adaptive overcurrent relays," in *Proc. IEEE Electr. Power Energy Conf. (EPEC)*, Oct. 2017, pp. 1–6.
[23] L. Chen, X. Tu, H. Chen, J. Yang, Y. Wu, X. Shu, and L. Ren, "Technical evaluation of superconducting fault current limiters used in a micro-grid by considering the fault characteristics of distributed generation, energy storage and power loads," *Energies*, vol. 9, no. 10, p. 769, Sep. 2016.
[24] Y. Zhang and R. A. Dougal, "State of the art of fault current limiters and their applications in smart grid," in *Proc. IEEE Power Energy Soc. Gen. Meeting*, Jul. 2012, pp. 1–6.
[25] K. A. Wheeler, M. Elsamahy, and S. O. Faried, "A novel reclosing scheme for mitigation of distributed generation effects on overcurrent protection," *IEEE Trans. Power Del.*, vol. 33, no. 2, pp. 981–991, Apr. 2018.
[26] P. M. Anderson, *Power System Protection*, 1st ed. Piscataway, NJ, USA: IEEE Press, 1999.
[27] M. Elsamahy, S. O. Faried, and T. S. Sidhu, "Impact of superconducting fault current limiters on the coordination between generator distance phase backup protection and generator capability curves," *IEEE Trans. Power Del.*, vol. 26, no. 3, pp. 1854–1863, Jul. 2011.
[28] *Distributed Energy Resources: Connection Modeling and Reliability Considerations*, NERC Document, North American Reliability Corporation (NERC), Atlanta, GA, USA, Feb. 2017.

MOHAMED ELSAMAHY (Member, IEEE) received the B.Sc. and M.Sc. degrees in electrical engineering from the Military Technical College (MTC), Cairo, Egypt, in 1997 and 2003, respectively, and the Ph.D. degree in electrical engineering from the University of Saskatchewan, Saskatoon, SK, Canada, in 2011. His research interests include power system protection and control, microgrids, integration of renewables, and sustainable energy systems, including nuclear power. He is a Registered Professional Engineer (P.Eng.) in Saskatchewan.